Journal of Molecular Graphics and Modelling 52 (2014) 71–81

Contents lists available at ScienceDirect

Journal of Molecular Graphics and Modelling

journal homepage: www.elsevier.com/locate/JMGM

A DFT study on the physical adsorption of cyclophosphamide derivatives on the surface of fullerene C_{60} nanocage

Zahra Shariatinia*, Samira Shahidi

Department of Chemistry, Amirkabir University of Technology, P.O. Box: 15875-4413, Tehran, Iran

ARTICLE INFO

Article history:
Accepted 7 June 2014
Available online 16 June 2014

Keywords:
DFT calculation
Fullerene
Anticancer drug
Cyclophosphamide
Physical adsorption

ABSTRACT

The physical sorption of a series of cyclophosphamide drug derivatives with formula $[NH(CH_2)_3O]P(O)(N[(CH_2)_xX]_2)$ where $x=2$, X = F (**2**), Cl (**3**), Br (**4**); $x=3$, X = F (**5**), Cl (**6**), Br (**7**) and $x=4$, X = F (**8**), Cl (**9**), Br (**10**) on the surface of fullerene C_{60} was studied using density functional theory (DFT) at B3LYP and B3PW91 levels. The most negative binding energies obtained using the B3LYP approach and corrected for geometrical BSSE and dispersion energies (gCP-D3-$\Delta E_{binding}$) were measured for compounds **8** (among isolated drugs) and **13** (among complexes). The dipole moments of isolated drugs were obtained close to those of their complexes with C_{60} (~4.0–5.5 Debye) indicating their hydrophililic nature that is an appropriate property appealing for drug delivery in biological media. The adsorption of all drugs on the surface of fullerene was endergonic with all of the $\Delta G_{adsorption} > 0$. The $\Delta H_{adsorption}$ values at B3PW91 level were only negative for complexes **14**–**16** indicating their exothermic adsorption nature. The HOMO–LUMO band gaps of complexes **11**–**19** were about 2.7 eV and are comparable with the gap in C_{60} but are much smaller than the gaps in isolated drugs **2**–**10** (6.5–8.0 eV) reflecting the increase in electrical conductivities upon complexation. The QTAIM data supported the covalent character of the C–O, C–N and N–H bonds, the intermediate character of P=O, P–O and P–N bonds while the electrostatic nature of P=O...C(fullerene) interactions. According to the gCP-D3-$\Delta E_{binding}$ binding energies and $\Delta H_{adsorption}$ values at B3LYP level, it seems that the complexes **12** and **13** can be the most promising prodrug + carrier delivery systems.

1. Introduction

Since the discovery of the "buckyball" (fullerene C_{60}) in 1985 as a stable allotrope of carbon with a closed cage structure [1] and then macroscopic scale synthesis of C_{60} [2], fullerenes have attracted great scientific interest for their possible applications especially as nanomaterial and biomedical species. It was found that fullerenes and their derivatives possess diverse medical applications and are promising as HIV inhibitor [3], photosensitive oxidizing agents against malignous skin cancer [4,5], Magnetic Resonance Imaging contrast agents [6], gene or drug delivery carriers [7,8] and neuroprotection by antioxidant activity for healing neurodegenerative illnesses [9]. Consequently, the potential exists that they can be used as drugs or carriers for various biological molecules.

Indeed, fullerene C_{60} has also received much attention because of its unique biological activities including toxicity and antioxidant capacity [10–13]. The biological activities of C_{60} are critically associated with its structure, concentration, stability and size distribution in aqueous media [14]. However, the fact that C_{60} is barely soluble in water give rises to suppressed biological activities [15]. As a result, several methods have been investigated for the preparation of water-soluble C_{60}, such as chemical modification [16], the formation of water-soluble host–guest complexes [17,18] or solubilization by surfactants [19,20].

The complexation of C_{60} with various compounds particularly cyclodextrins [18,21], porphyrines [22], metalloporphyrines [23] and calixarenes [24,25] have been performed to increase the fullerene solubility. Fullerene-based low toxic nanocationite particles that are porphyrin adducts of cyclohexyl fullerene-C_{60} were used to treat hypoxia-induced mitochondrial dysfunction in mammalian heart muscle [26]. It has been revealed that nano-sized clusters of a teicoplanin ψ-aglycon-fullerene conjugate exhibit antibacterial activity against enterococci resistant to teicoplanin [27].

Various computational approaches have frequently been done on the interaction between fullerenes and different species [28–30].

* Corresponding author. Tel.: +98 2164542766; fax: +98 2164542762.
E-mail addresses: shariati@aut.ac.ir, shariatiz@yahoo.com (Z. Shariatinia).

http://dx.doi.org/10.1016/j.jmgm.2014.06.001
1093-3263/

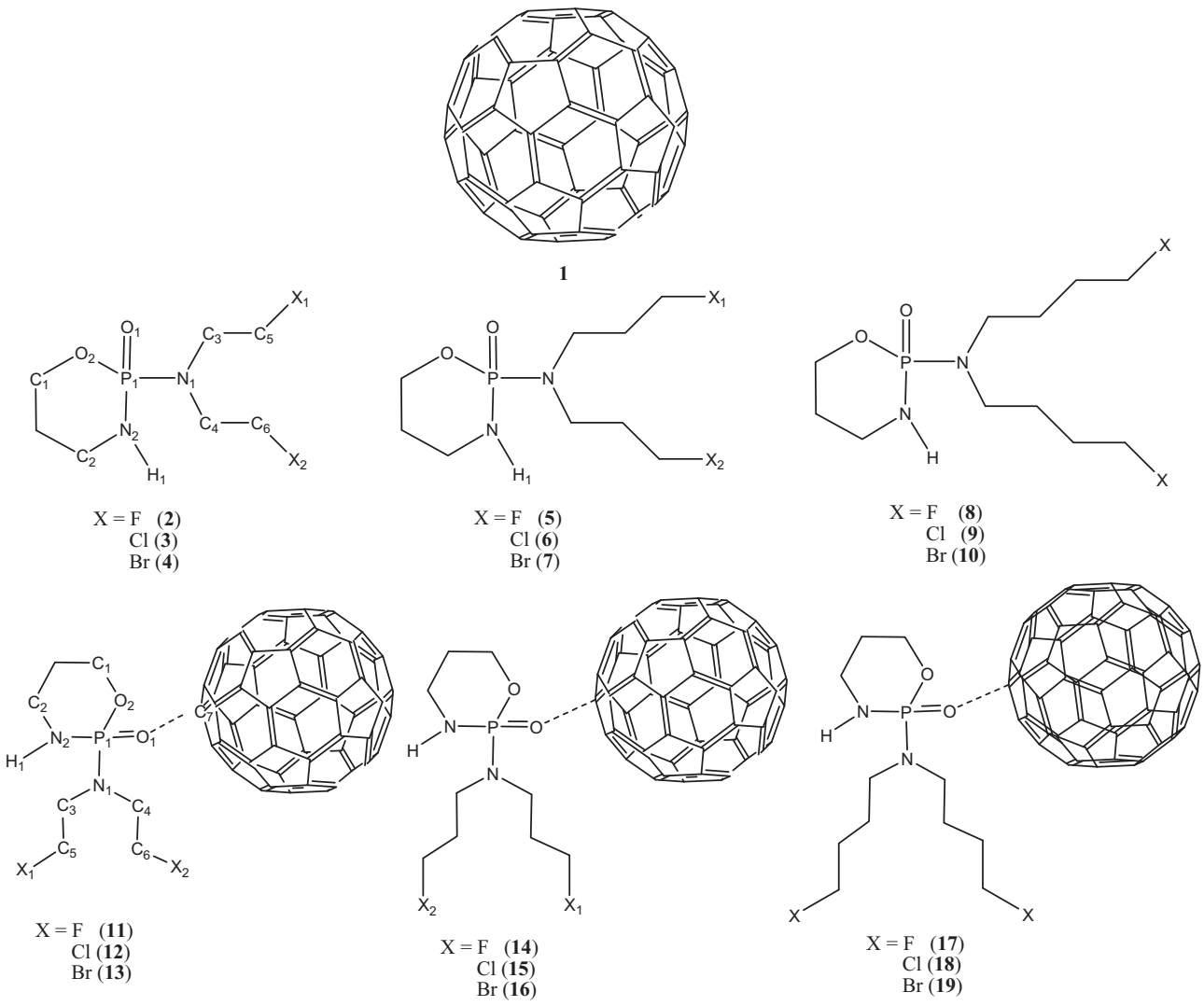

Scheme 1. The molecular structures of compound **1**–**19**. The atom-labeling schemes are shown for compounds **2**–**4** and **11**–**13**.

First-principles density functional and quantum Monte Carlo calculations on light-element B and Be doped fullerenes displayed significantly enhanced molecular H_2 binding [31]. Cyclophosphamide (CP, CAS 50-18-0) is a well-known anticancer prodrug that is activated by cytochrome P-450 in the liver [32] and indicates therapeutic activity against numerous human cancers [33–36]. Literature review indicates that there is not any report about the adsorption of cyclophosphamide on the fullerene surface.

The aim of this work is to predict the structural and electronic properties of complexes formed between nine physically adsorbed anticancer prodrug analogs of cyclophosphamide and fullerene C_{60} (as a drug carrier). For this purpose, DFT computations were conducted at B3LYP and B3PW91 levels on 19 compounds including isolated drugs and also their complexes with C_{60} nanocage.

2. Computational details

The structures of compounds **1**–**19** (Scheme 1) were drawn and optimized in Hyperchem 7.0 program suite. Also, log *P* values were computed in Hyperchem to evaluate the lipophilicity of these molecules. The quantum chemical calculations were performed to fully optimize the geometries of the structures by Gaussian 98 program [37] using density functional theory (DFT) at B3LYP and B3PW91 levels and standard 6-31G(d) basis set. The gCP-D3 energy corrections to B3LYP method were directly obtained on a web service created by Professor Stefan Grimme (http://wwwtc.thch.uni-bonn.de/).

The optimizations were followed by computations of the harmonic and the vibrational frequencies, so that no imaginary frequencies were obtained at these computations. The natural bond orbital (NBO) calculations were performed to obtain the HOMO, LUMO and band gap energies, the Wiberg bond orders, electron density charge transfers and their energies, atomic hybridizations as well as natural atomic charges. Nuclear quadrupole coupling constants (χ) were calculated from the equation $\chi = e^2 q_{zz} Q/h$ [38], supposing the electric quadrupole moments (Q) of ^{2}H (I = 1), ^{17}O (I = 5/2), ^{14}N (I = 1), ^{35}Cl (I = 3/2), ^{37}Cl (I = 3/2), ^{79}Br (I = 3/2) and ^{81}Br (I = 3/2) nuclei are 2.86, 25.58, 20.44, −81.65, −64.35, 313 and 261.5 mb (1 mb = 10^{-31} m^2), respectively [39]. The principal components of the EFG tensor, q_{ii}, are computed in atomic units (1 au = 9.717365 × 10^{21} V m^{-2}), with $|q_{zz}| \geq |q_{yy}| \geq |q_{xx}|$ and $q_{xx} + q_{yy} + q_{zz} = 0$. These diagonal elements are related to each other by the asymmetry parameter: $\eta = |q_{yy} - q_{xx}|/|q_{zz}|$, $0 \leq \eta \leq 1$, which measures the EFG tensor deviation from axial symmetry. The computed q_{zz} component of EFG tensor is used to obtain the nuclear quadrupole coupling constants (χ).

Table 1
The binding energies ($\Delta E_{binding}$, kcal/mole), dipole moments (Debye), band gaps ($E_g = E_{HOMO} - E_{LUMO}$, eV) and log *P* for compounds **11–19**.

No.	Compound	$\Delta E_{binding}$	[a]gCP-D3-$\Delta E_{binding}$	$\Delta E_{binding}$	Dipole moment		E_g		Log *P*
		B3LYP	B3LYP	B3PW91	B3LYP	B3PW91	B3LYP	B3PW91	
11	Full-F	−1.6533	−7.0555	−0.8978	4.8907	4.6849	2.739	2.743	−0.09
12	Full-Cl	−3.6365	−9.5080	−0.7310	4.4045	4.8503	2.733	2.743	1.00
13	Full-Br	−3.5721	−9.5504	−0.7016	4.2774	4.8131	2.742	2.745	1.13
14	Full-F2	−4.2523	−7.4942	−2.0780	3.8562	4.8384	2.742	2.739	0.02
15	Full-Cl2	−2.4395	−7.7662	−1.3151	4.3028	4.4219	2.737	2.740	1.10
16	Full-Br2	−4.1087	−7.3045	−2.7380	5.5684	4.6285	2.745	2.745	1.23
17	Full-F3	−1.0757	−6.9421	0.1835	5.6807	4.4347	2.742	2.741	0.92
18	Full-Cl3	−0.6200	−5.2588	0.1741	4.4360	4.5025	2.740	2.743	2.01
19	Full-Br3	−1.4363	−8.1796	0.1340	4.2295	4.5212	2.739	2.743	2.13

[a] Corrected binding energy for dispersion and courterpoise energies (gCP-D3).

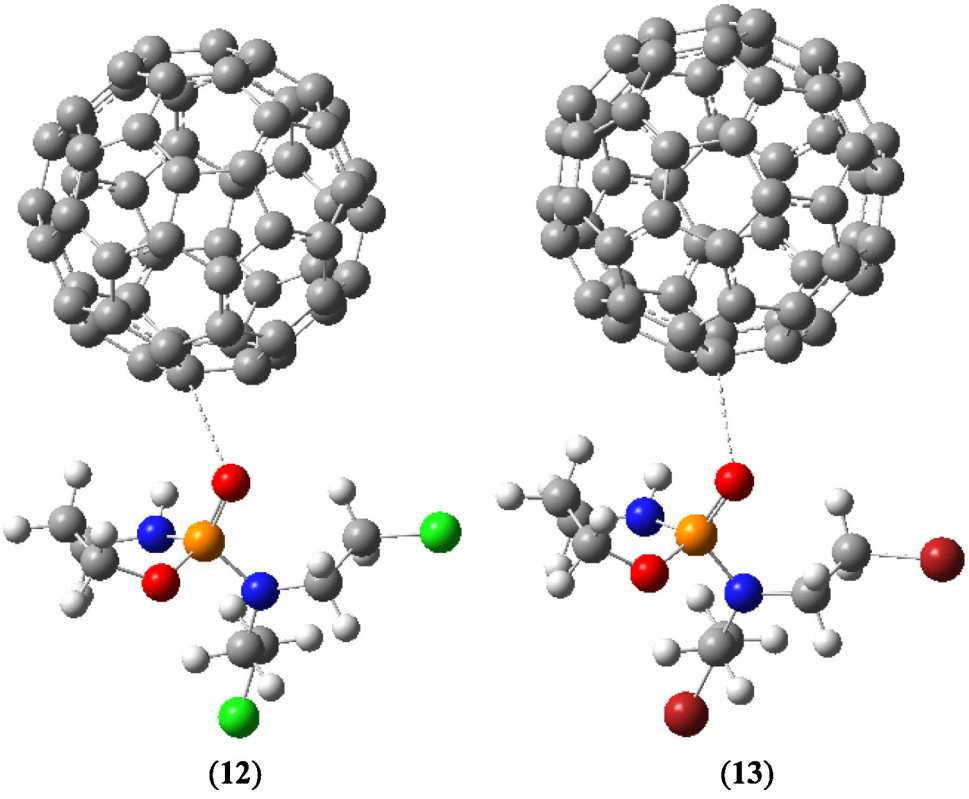

Fig. 1. The optimized structures of compounds **12** and **13** at B3LYP/6-31G(d) level.

Topological analysis of electron density for the optimized structures of compounds **1–19** at both B3LYP and B3PW91 levels were performed using the Quantum Theory of Atoms in Molecules (AIM) of Bader [40]. The QTAIM analysis was concentrated on the B3LYP and B3PW91 calculated wave functions of electron densities obtained for the optimized structures of compounds **1–19**. The resulting wave function files were used as inputs to AIM2000 program [41] for calculating the topological properties of electron

Table 2
The relative Gibbs free energies, $\Delta G_{adsorption}$, relative enthalpies and $\Delta H_{adsorption}$ for compounds **11–19**.

No.	Compound	Relative Gibbs free energy		$\Delta G_{adsorption}$ (kcal/mol)		Relative enthalpy		$\Delta H_{adsorption}$ (kcal/mol)	
		B3LYP	B3PW91	B3LYP	B3PW91	B3LYP	B3PW91	B3LYP	B3PW91
11	Full-F	0.3583	0.3575	11.1651	8.9130	5100.90	5100.88	−1.0235	0.4851
12	Full-Cl	0.3520	0.3556	10.4968	10.8670	4380.15	4380.17	−2.2515	0.0502
13	Full-Br	0.3484	0.3483	10.3782	8.5604	157.13	157.08	−2.2226	0.6150
14	Full-F2	0.4094	0.4100	10.0287	8.4964	5022.33	5022.34	−2.9612	−0.7511
15	Full-Cl2	0.4035	0.4063	9.4966	9.1565	4301.59	4301.63	−1.2556	−0.0163
16	Full-Br2	0.4040	0.4050	12.3624	10.7321	78.56	78.54	−2.7811	−1.3968
17	Full-F3	0.4625	0.4643	9.8367	9.0993	4943.76	4943.80	0.1939	1.5939
18	Full-Cl3	0.4575	0.4600	10.1749	9.6484	4223.02	4223.09	0.8013	1.6547
19	Full-Br3	0.4551	0.4565	10.6091	9.6164	0	0	−0.1142	1.5750

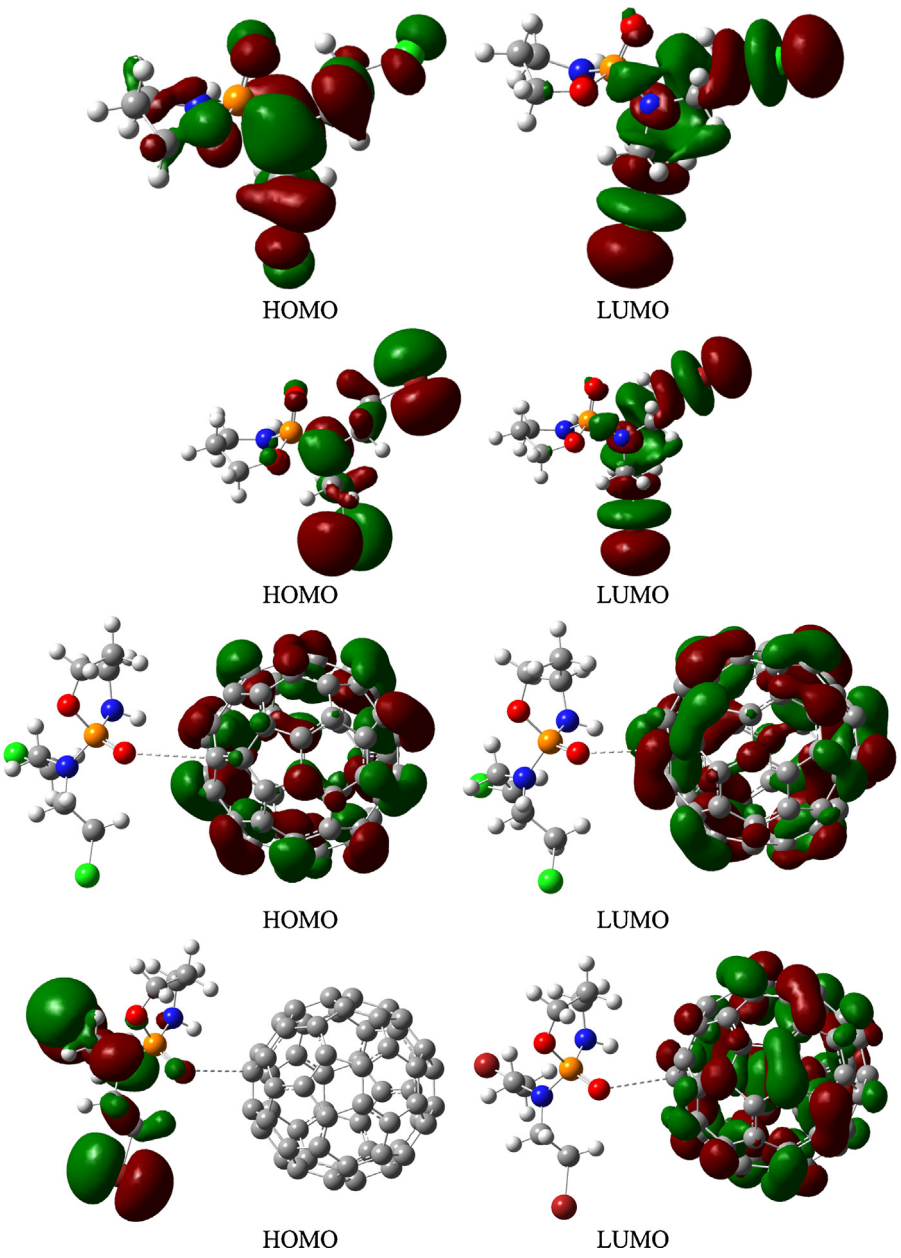

Fig. 2. The HOMO and LUMO molecular orbitals of compounds **3**, **4**, **12** and **13** at B3LYP/6-31G(d) level (from top to down, respectively). Red and green represent negative and positive regions of the wave functions, respectively.

densities and their Laplacian. Considering the local Virial theorem, the following characteristics of bond critical points (bcps) were taken into account: electron density at BCPs, $\rho(\mathbf{r})$, their Laplacian, $\nabla^2\rho(\mathbf{r})$, the electronic kinetic energy density, $G(\mathbf{r})$, the electronic potential energy density, $V(\mathbf{r})$, and the total electronic energy density, $H(\mathbf{r})$. These properties have been employed as useful indicators for evaluating the nature of bonds (covalent, electrostatic, hydrogen bonding and so on) and also for quantitative

Table 3
The selected Wiberg bond orders for compounds **2**–**4**.

Bond	**2**		**3**		**4**	
	B3LYP	B3PW91	B3LYP	B3PW91	B3LYP	B3PW91
P1–O1	1.2789	1.2834	1.2795	1.2827	1.2748	1.2766
P1–O2	0.6741	0.6756	0.6785	0.6791	0.6798	0.6817
P1–N1	0.7530	0.7518	0.7461	0.7460	0.7472	0.7459
P1–N2	0.7677	0.7714	0.7687	0.7737	0.7683	0.7739
O2–C1	0.8712	0.8747	0.8686	0.8725	0.8696	0.8732
N1–C3	0.9475	0.9477	0.9447	0.9448	0.9419	0.9416
N1–C4	0.9543	0.9548	0.9516	0.9519	0.9486	0.9490
N2–C2	0.9661	0.9679	0.9647	0.9666	0.9650	0.9667
N2–H1	0.7939	0.7861	0.7941	0.7862	0.7946	0.7867

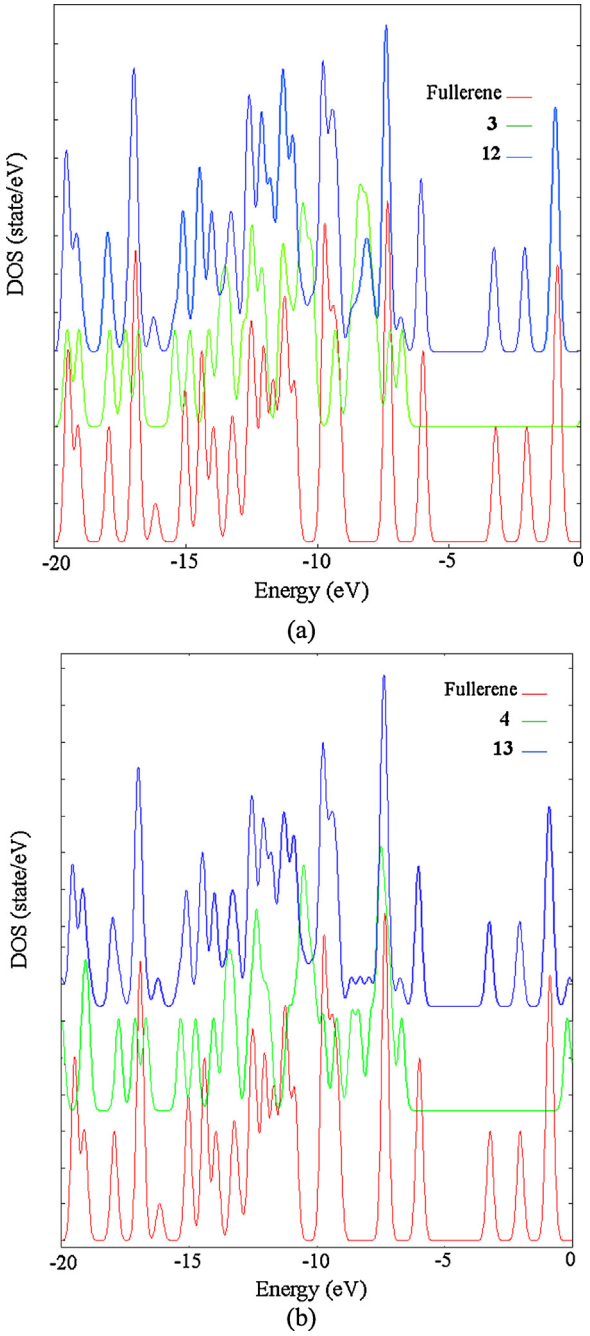

Fig. 3. The density of state (DOS) spectra of fullerene C_{60}, compounds **3**, **12** and **4**, **13** at B3LYP/6-31G(d) level (a and b, respectively).

representation of interatomic interactions in compounds **1**–**19**.

3. Results and discussion

3.1. Optimization and energies of the structures

In order to investigate the electronic and structural properties of isolated fullerene C_{60} (**1**) and various derivatives of cyclophosphamide prodrug (**2**–**10**) as well as those of their related complexes **11**–**19** (Scheme 1), DFT computations were performed at B3LYP and B3PW91 levels of theory using 6-31G(d) basis set. The binding energies for the isolated and complex compounds were calculated from the equations $\Delta E_{binding} = E(\text{molecule}) - \Sigma_i E(i)$, i = atom or ion and $\Delta E_{binding} = E(\text{complex}) - \Sigma E[(\text{drug molecule}) + E(\text{fullerene})]$, respectively. The $\Delta E_{binding}$ values obtained using B3LYP method were corrected by addition of geometrical counterpoise (gCP) and dispersion (D3) energies to the $\Delta E_{binding}$ binding energies as gCP-D3-$\Delta E_{binding}$. The gCP energy corrects the intramolecular basis set superposition error and the D3 energy corrects the dependence of the London dispersion interaction energy on the inter-atomic/molecular distance for the weak and non-covalent interactions [42].

The $\Delta E_{binding}$/gCP-D3-$\Delta E_{binding}$ values (kcal/mol) for compounds **11**–**19** are given in Table 1 and those of **1**–**10** in Table S1. It is notable that applying gCP-D3 correction energies to the binding energies considerably affects the $\Delta E_{binding}$ values. It can be seen that among compounds **2**–**4** that only differ in the halogen atoms of the C–X bond (X = F, Cl, Br), compound **2** is the most stable one at both B3LYP and B3PW91 levels with the most negative $\Delta E_{binding}$. Comparing similar compounds **5**–**7** and **8**–**10** reveals identical results in which the fluoro derivatives are the most stable compounds. Among compounds **2**, **5** and **8**, compound **8** indicates the most negative $\Delta E_{binding}$ that can be related to its longer aliphatic chain.

The gCP-D3-$\Delta E_{binding}$ for the isolated compounds **1**–**10** using the B3LYP method changes in the order of F3 (**8**) > Cl3 (**9**) > Br3 (**10**) > F2 (**5**) > Cl2 (**6**) > Br2 (**7**) > F (**2**) > Cl (**3**) > Br (**4**) reflecting among analogous compounds, the larger molecules produce greater $\Delta E_{binding}$. This trend is not observed when comparing the $\Delta E_{binding}$ for complexes **11**–**19** at the B3LYP level for which the order of gCP-D3-$\Delta E_{binding}$ is Full-Br (**13**) > Full-Cl (**12**) > Full-Br3 (**19**) > Full-Cl2 (**15**) > Full-F2 (**14**) > Full-Br2 (**16**) > Full-F (**11**) > Full-F3 (**17**) > Full-Cl3 (**18**). Obviously, there is no regular variation in $\Delta E_{binding}$ of complexes. Moreover, the most negative binding energies are obtained for complexes **13** and **12** (−9.5504 and −9.5080 kcal/mol), respectively. The above orders for the gCP-D3-$\Delta E_{binding}$ reflect that the energy of a system is a complex parameter depending on different factors including basis set, size of molecule, nature of atoms, stereochemistry and so forth. Accordingly, a regular trend is not observed for the energy change even in a series of such very analogous derivatives.

The optimized structures of the most stable complexes **12** and **13** at B3LYP level are presented in Fig. 1 displaying the physical adsorption of each drug through its phosphoryl oxygen atom onto a carbon atom of fullerene C_{60} nanocage. It can be observed that none of the aliphatic six-membered rings demonstrate a chair conformations but they have a boat conformation. This is interesting, because the crystal structures of similar diazaphosphorinanes in which there are N–P–N moieties within the aliphatic six-membered ring reveal chair conformations [43].

Calculated dipole moments (μ, Debye) for compounds **11**–**19** are given in Table 1 and those of molecules **1**–**10** in Table S1. The data indicate relatively the same values at both B3LYP and B3PW91 methods. Among these compounds, C_{60} does not show any polarity with $\mu = 0$, but compound **10** reveals the greatest μ (5.2946 D). It is interesting that the dipole moments of isolated drugs are comparable with those of their related complexes with C_{60} (~4.0–5.5 Debye). This result illustrates that adsorption of drugs on C_{60} enhances the polarity of the whole system which is a desired property for drug delivery in biological media.

It has been pointed out that lipophilicity is an important factor for biochemical, pharmacological and environmental processes in quantitative structure–activity relationship (QSAR) studies [44]. Thus, to evaluate the lipophilicities of compounds **1**–**19**, their log P values were computed using Hyperchem software to predict their toxicities, Table 1 and S1. The log P values which correspond to log(1/IC_{50}) reveal that compounds **9** and **10** can be the most toxic molecules with the greatest log P values (≈4.0). It can be

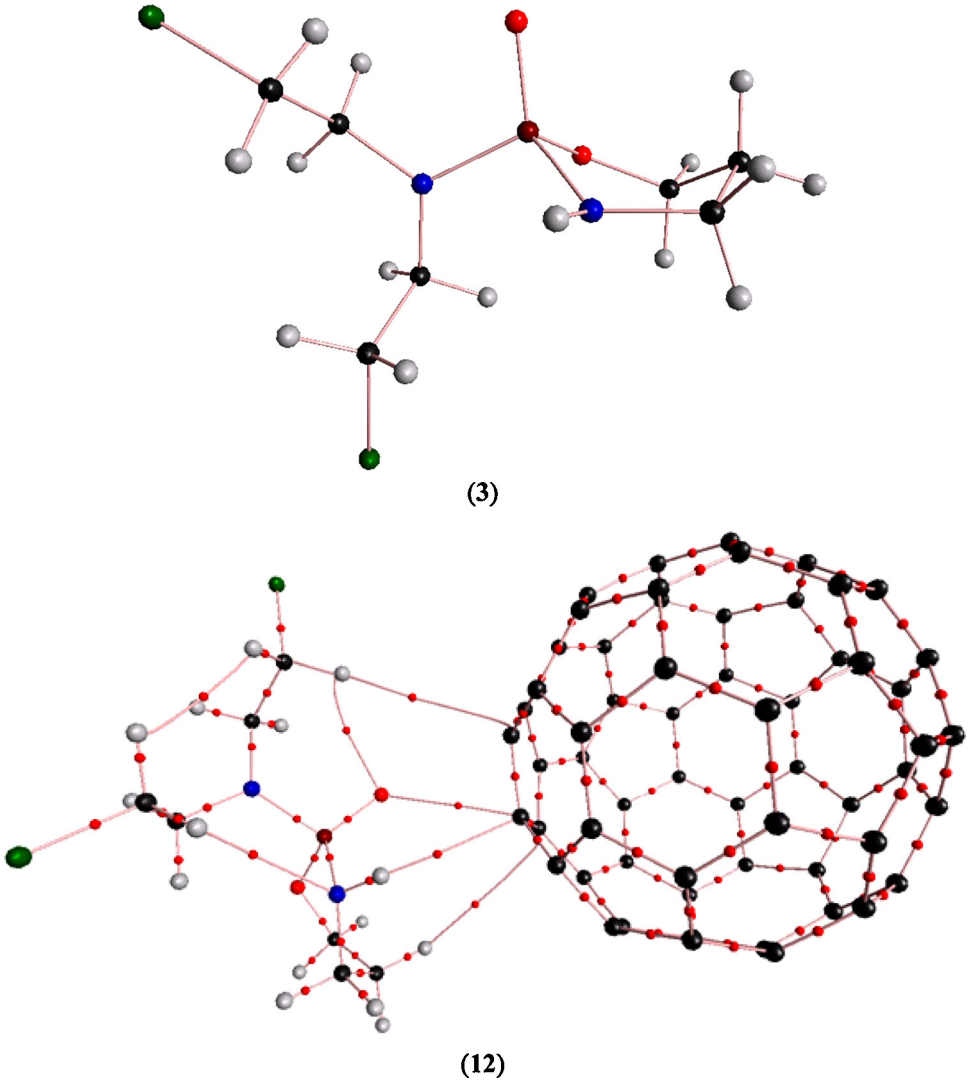

Fig. 4. The molecular graphs (MGs) of compounds **3** and **12** obtained by QTAIM analysis at B3LYP/6-31G(d) level of theory. Bond critical points: red circles; Bond paths: pink lines. (For interpretation of the references to color in this figure legend, the reader is referred to the web version of the article.)

seen that the size of a molecule is the most important parameter (steric effect) affecting the log *P* except for fullerene C_{60} that indicates log *P* = 0. That is, with increasing the size of a molecule in closely related structures (compounds **2**–**4**, **5**–**7**, **8**–**10**, **11**–**13**, **14**–**16** and **17**–**19**), log *P* increases. Furthermore, the lipophilicities of isolated drug molecules **2**–**10** are greater than those of their related complexes **11**–**19**. This is owing to the interactions of drugs with C_{60} that has a log *P* = 0. The lipophilicity of thermodynamically the most stable compounds **12** and **13** are close to each other with their log *P* values equal to 1.00 and 1.13, respectively.

The relative Gibbs free energies, Gibbs free energies of adsorption ($\Delta G_{adsorption}$), relative enthalpies and enthalpies of adsorption ($\Delta H_{adsorption}$) for compounds **1**–**10** and **11**–**19** are given in Tables S2 and 2, respectively. The $\Delta G_{adsorption}$ and $\Delta H_{adsorption}$ were calculated using the following equations.

$$\Delta G_{adsorption} = G(\text{drug-fullerene complex}) - \Sigma G(\text{drug}) + G(\text{fullerene})$$

$$\Delta H_{adsorption} = H(\text{drug-fullerene complex}) - \Sigma H(\text{drug}) + H(\text{fullerene})$$

It can be observed from these tables that comparable results are obtained at both B3LYP and B3PW91 levels and the adsorption process for all drugs on the surface of fullerene is endergonic (all $\Delta G_{adsorption} > 0$) that means these are non-spontaneous reactions. The relative Gibbs free energies are in the range of 0 (for **4**) to 0.4625 (for **17**) and relative enthalpies change from 0 (for **19**) to 7308.11 (for **5**) when B3LYP method is used. The $\Delta H_{adsorption}$ values are negative only for compounds **11**–**16**, **19** and **14**–**16** at B3LYP and B3PW91 levels, respectively, reflecting their exothermic reaction behavior. The positive signs for the $\Delta H_{adsorption}$ of other complexes prove that their adsorption process is endothermic. The $\Delta G_{adsorption}$ and $\Delta H_{adsorption}$ vary in the range of 9.8367–12.3624 and −2.9612 to 0.8013 kcal/mol, respectively. It is notable that adsorptions of the most stable complexes **12**, **13** are both exothermic at B3LYP method.

Selected bond lengths and angles of compounds **2**–**4** and **11**–**13** are listed in Table S3. The P1–O1 and P1–O2 bond lengths in all compounds are about 1.49, 1.63 Å, respectively, that are close to the P=O double bond (1.45 Å) and P–O single bond (1.64 Å) lengths [45]. The smaller P1–O1 bond lengths in comparison with P1–O2 bond lengths exhibit the greater bond order for the phosphoryl bond. Moreover, in complexes **11**–**13**, the P1–O1 bond lengths at B3LYP level are 1.4883, 1.4887, 1.4888 Å that are very slightly longer than those of isolated drug molecules **2**–**4** (1.4868, 1.4866, 1.4866 Å), respectively, that is due to the physical adsorption of drugs onto the fullerene C_{60} surface. The Wiberg bond orders for compounds **2**–**4** are given in Table 3 indicating nearly identical values using both the B3LYP and B3PW91 approaches. Comparing the P1–O1

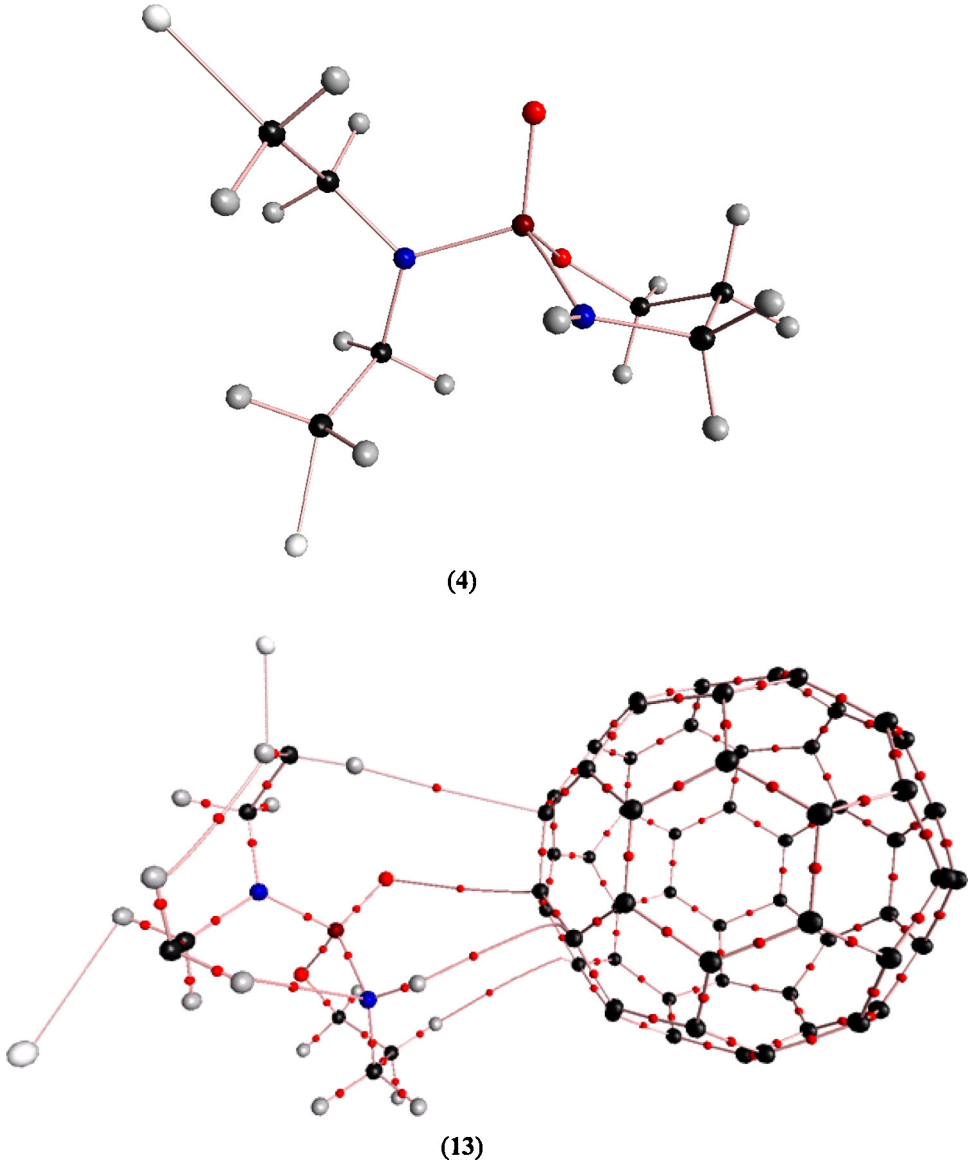

Fig. 5. The molecular graphs (MGs) of compounds **4** and **13** obtained by QTAIM analysis at B3LYP/6-31G(d) level of theory. Bond critical points: red circles; Bond paths: pink lines. (For interpretation of the references to color in this figure legend, the reader is referred to the web version of the article.)

and P1–O2 bond lengths reflects their approximately double and single bond characters and confirms much greater bond orders for the P1–O1 bonds.

In these molecules, the P1–N1 and P1–N2 bond lengths are about 1.67, 1.69 Å, respectively, that are shorter than the P–N single bond length (1.77 Å [45]). This can be attributed to the existence of partial multiple bond character in these bonds. The slightly smaller P–N bond for the exocyclic groups may be owing to the electron donation of halogen atoms through resonance effect leading to the more interaction of nitrogen lone pair with the phosphorus atom. Similar results were also obtained for some previously reported phosphoramides [43,46]. All of the C–O and C–N bond lengths are about 1.44, 1.47 Å, respectively. The C–X bonds are near 1.39, 1.82, 1.99 Å for X = F, Cl, Br, respectively, indicating smaller C–X bond for the smaller, more electronegative halogen atom. The equilibrium distance measured from the phosphoryl oxygen and fullerene carbon atom at B3LYP level of theory in complexes **11**–**13** are 3.3144, 3.3724, 3.25690 Å, respectively, reflecting an interaction (physisorption) exists between each drug and C_{60} in all complexes.

In molecules **2**–**19**, the phosphorus atoms indicate distorted tetrahedral configurations. For example, the angles around P1 atom in **3** vary from 100.46° to 119.64° at B3LYP/6-31G(d) method. In these molecules, the environments of endocyclic N2 nitrogen atoms are deviated from planarity, but the exocyclic N1 atoms are almost planar. In compound **3**, for instance, the angles P1–N2–C2, P1–N2–H1 and C2–N2–H1 are 121.27°, 112.36° and 113.23°, respectively, with average of 115.62°. The sum of surrounding angles around N1 atom is 357.81° with the average of 119.27° indicating its planarity. The deviation of endocyclic nitrogen atom from planarity can be ascribed to the ring starin on the bonds that causes their deviation. The observation suggests existence of partial multiple bond character between phosphorus and nitrogen atoms that has always been confirmed by the crystallographic data of our previous similar compounds [43,46].

3.2. NBO analysis

The band gaps (E_g) of compounds **1**–**19** which are the differences of energies between the HOMO (highest occupied molecular

Table 4
The electron density ($\rho(\mathbf{r})$ in ea_0^{-3}), Laplacian of electron density ($\nabla^2\rho(\mathbf{r})$ in ea_0^{-5}), kinetic energy density ($G(\mathbf{r})$ in $e^2a_0^{-4}$), potential energy ($V(\mathbf{r})$ in $e^2a_0^{-4}$), total electronic energy density ($H(\mathbf{r})$ in $e^2a_0^{-4}$) and $|V(\mathbf{r})|/G(\mathbf{r})$ calculated by QTAIM method at B3LYP/6-31G(d) level for bond paths in compounds **3**, **4**, **12** and **13**.

Bond	$\rho(\mathbf{r})$	$\nabla^2\rho(\mathbf{r})$	$G(\mathbf{r})$	$V(\mathbf{r})$	$H(\mathbf{r})$	$\lvert V(\mathbf{r})\rvert/G(\mathbf{r})$
3						
P1–O1	0.2263	1.6004	0.5514	−0.7028	−0.1514	1.2745
P1–O2	0.1667	0.7360	0.2920	−0.4000	−0.1080	1.3698
P1–N1	0.1750	0.4901	0.2634	−0.4042	−0.1408	1.5348
P1–N2	0.1727	0.4562	0.2534	−0.3927	−0.1393	1.5498
O2–C1	0.2340	−0.3795	0.2195	−0.5339	−0.3144	2.4322
N1–C3	0.2537	−0.6811	0.1190	−0.4083	−0.2893	3.4307
N2–C2	0.2515	−0.6683	0.1125	−0.3920	−0.2795	3.4855
N2–H1	0.3267	−1.5983	0.0498	−0.4992	−0.4494	10.0228
4						
P1–O1	0.2263	1.5994	0.5512	−0.7025	−0.1513	1.2746
P1–O2	0.1667	0.7361	0.2921	−0.4001	−0.1080	1.3699
P1–N1	0.1750	0.4912	0.2635	−0.4042	−0.1407	1.5339
P1–N2	0.1726	0.4538	0.2527	−0.3920	−0.1393	1.5511
O2–C1	0.2341	−0.3798	0.2198	−0.5346	−0.3148	2.4320
N1–C3	0.2533	−0.6777	0.1195	−0.4083	−0.2889	3.4183
N2–C2	0.2515	−0.6682	0.1125	−0.3920	−0.2795	3.4853
N2–H1	0.3266	−1.5978	0.0498	−0.4991	−0.4493	10.0151
12						
P1–O1	0.2250	1.5816	0.5455	−0.6955	−0.1501	1.2751
P1–O2	0.1672	0.7486	0.2953	−0.4034	−0.1081	1.3661
P1–N1	0.1766	0.5042	0.2683	−0.4147	−0.1422	1.5301
P1–N2	0.1748	0.4512	0.2556	−0.3984	−0.1428	1.5587
O2–C1	0.2311	−0.3823	0.2099	−0.5153	−0.3054	2.4554
N1–C3	0.2545	−0.6861	0.1206	−0.4127	−0.2921	3.4221
N2–C2	0.2518	−0.6667	0.1112	−0.3891	−0.2779	3.4991
N2–H1	0.3256	−1.5997	0.0489	−0.4978	−0.4489	10.1720
PO1…C7	0.0047	0.0172	0.0034	−0.0026	−0.0008	0.7545
CH.HC	0.0048	0.0175	0.0032	−0.0021	0.0011	0.6530
CH…NH	0.0062	0.0215	0.0045	−0.0036	0.0009	0.8082
ClCH…C(fullerene)	0.0014	0.0044	0.0008	−0.0004	0.0003	0.5758
N2-H…C(fullerene)	0.0070	0.0224	0.0044	−0.0032	0.0012	0.7326
CH…C(fullerene)	0.0018	0.0052	0.0010	−0.0006	0.0004	0.6287
13						
P1–O1	0.2250	1.5820	0.5454	−0.6953	−0.1499	1.2748
P1–O2	0.1673	0.7514	0.2958	−0.4038	−0.1080	1.3650
P1–N1	0.1765	0.5048	0.2681	−0.4101	−0.1419	1.5294
P1–N2	0.1746	0.4529	0.2557	−0.3983	−0.1425	1.5573
O2–C1	0.2312	−0.3806	0.2108	−0.5167	−0.3059	2.4514
N1–C3	0.2542	−0.6839	0.1214	−0.4138	−0.2924	3.4081
N2–C2	0.2518	−0.6670	0.1115	−0.3898	−0.2783	3.4954
N2–H1	0.3257	−1.6004	0.0489	−0.4979	−0.4490	10.1820
PO1…C7	0.0059	0.0202	0.0042	−0.0033	0.0009	0.7879
CH.HC	0.0050	0.0183	0.0034	−0.0022	0.0012	0.6517
CH…NH	0.0069	0.0227	0.0048	−0.0040	0.0009	0.8234
BrCH…C(fullerene)	0.0012	0.0039	0.0007	−0.0004	0.0003	0.5712
N2–H…C(fullerene)	0.0064	0.0197	0.0039	−0.0028	0.0011	0.7225
CH…C(fullerene)	0.0024	0.0069	0.0013	−0.0008	0.0004	0.6550

orbital) and LUMO (lowest unoccupied molecular orbital) and are measures of electron conductivities are given in Table 1 and S1. It is observed that the band gaps of pristine C_{60} (**1**) and complexes **11**–**19** (∼2.7 eV) are almost identical while those of isolated drugs **2**–**10** are very much higher in the range of about 6.5–8.0 eV. This indicates the great increase in electrical conductivities of the drugs upon complexation. The very slightly smaller band gaps of complexes (∼0.02 eV) compared with that of C_{60} can be related to the interaction between the drugs and C_{60}.

The HOMO and LUMO molecular orbitals of drugs **3**, **4** and their corresponding complexes **12**, **13** are depicted in Fig. 2. It is clear that the electron density in HOMO of **3** is almost on all atoms of the molecule while for the LUMO orbital, the electron density is mostly on the $N[(CH_2)_2Cl]_2$ moiety. In compound **4**, the electron densities of HOMO and LUMO orbitals are located especially on the $N[(CH_2)_2Br]_2$ group. The HOMO and LUMO orbitals of **12** are entirely located on the fullerene C_{60} and there is nothing within the interacting distances. Interestingly, the HOMO orbital of **13** illustrates that the electron density has been placed on $N[(CH_2)_2Br]_2$ moiety of drug. The LUMO orbital of **13** is again exists only on C_{60}.

The natural atomic charges for compounds **2**–**4** and **11**–**13** are presented in Table S4. It is observed that the phosphorus atoms have positive charges but the oxygen and nitrogen atoms have negative charges with the O1 atoms show the most negative charges. The carbon atoms connected to the fluorine atoms indicate positive charges while those bonded to Cl and Br atoms reveal positive charges. The negative charges on fluorine atoms (∼−0.38 e) are very much higher than those on Cl (∼−0.09 e) and Br (∼−0.04 e) nuclei. The carbon atom of C_{60} to which the phosphoryl oxygen is bonded display positive charge (∼0.02 e). The presence of small positive charge on the carbon atom of C_{60} connected to the O1 suggests physical interaction between the drugs and C_{60}.

Table S5 presents the atomic hybridizations for compounds **3**, **4**, **12** and **13** at B3LYP/6-31G(d) level. The phosphorus hybridization in **3** for P1–O1, P1–O2 and P1–N1 bonds are $sp^{2.51}d^{0.31}$, $sp^{2.21}d^{1.54}$ and $sp^{2.07}d^{1.15}$, respectively. Therefore, the phosphorus atom has a nearly sp^2d hybridization instead of sp^3 in these bonds. The oxygen and nitrogen atoms all indicate almost sp^2 hybridization but the carbon, chlorine and bromine atoms exhibit nearly $sp^{4.5}d^{0.01}$ (or $sp^{5.5}d^{0.01}$), $sp^{5.5}d^{0.03}$ and $sp^{7.5}d^{0.05}$ hybridizations, respectively.

Table 5
Calculated nuclear quadrupole coupling constants (NQCC, χ) and asymmetry parameter (η) for ^{2}H (kHz) and ^{17}O, ^{14}N, $^{35/37}$Cl, $^{79/81}$Br (MHz) nuclei of compounds **3**, **4**, **12** and **13**.

Compound	χ		η		Compound	χ		η	
	B3LYP	B3PW91	B3LYP	B3PW91		B3LYP	B3PW91	B3LYP	B3PW91
3					**4**				
O1	4.9389	4.8850	0.0671	0.0419	O1	4.9400	4.8841	0.0657	0.0452
O2	9.7457	9.7031	0.6738	0.6825	O2	9.7383	9.6862	0.6741	0.6789
N1	5.3071	5.2033	0.1309	0.1321	N1	5.2727	5.1826	0.1267	0.1293
N2	4.9241	4.8406	0.1511	0.1548	N2	4.9189	4.8229	0.1506	0.1539
H1	255.22	258.90	0.1811	0.1767	H1	255.11	258.78	0.1807	0.1759
^{35}Cl1	294.29	296.02	0.0203	0.0211	^{79}Br1	2096.65	2100.34	0.0270	0.0278
^{35}Cl2	293.23	293.98	0.0259	0.0267	^{79}Br2	2088.43	2086.79	0.0322	0.0331
^{37}Cl1	231.93	233.30	0.0203	0.0211	^{81}Br1	1751.68	1754.76	0.0270	0.0278
^{37}Cl2	231.10	231.69	0.0259	0.0267	^{81}Br2	1744.81	1743.44	0.0322	0.0331
12					**13**				
O1	4.9820	4.9331	0.1734	0.0476	O1	4.9697	4.9276	0.1875	0.0569
O2	9.3188	9.6792	0.6698	0.6715	O2	9.3288	9.6770	0.6646	0.6743
N1	5.4078	5.2136	0.1333	0.1326	N1	5.3730	5.1927	0.1292	0.1272
N2	4.8101	4.8318	0.1772	0.1487	N2	4.8342	4.8168	0.1769	0.1511
H1	247.99	258.96	0.1866	0.1770	H1	248.18	258.76	0.1866	0.1762
^{35}Cl1	291.97	296.21	0.0212	0.0212	^{79}Br1	2077.16	2102.31	0.0275	0.0280
^{35}Cl2	291.73	294.33	0.0257	0.0262	^{79}Br2	2078.61	2090.17	0.0318	0.0327
^{37}Cl1	230.11	233.45	0.0212	0.0212	^{81}Br1	1735.39	1756.41	0.0275	0.0280
^{37}Cl2	229.92	231.97	0.0257	0.0262	^{81}Br2	1736.60	1746.26	0.0318	0.0327

The fullerene carbon atom engaging in the weak interaction with drug illustrates a ~sp^2 hybrid.

To further interpret the nature of the binding in these systems, the electronic structures of the thermodynamically most stable states between drugs **3**, **4** and C_{60} in compounds **12** and **13** were studied. For this purpose, their density of states (DOS) spectra were calculated and indicated in Fig. 3. It is clearly observed that there are some hybridization between the C_{60} and the each drug molecule. Consequently, the existence of interactions is deduced quantitatively in terms of the DOS spectra.

The interaction energies from the NBO perturbation theory energy analysis for the transitions from oxygen/nitrogen lone pairs to the vicinal antibonding orbitals or from a bonding σ/π orbital to a vicinal antibonding σ^*/π^* orbital in compounds **3**, **4**, **12** and **13** are presented in Table S6. It can be seen that very similar results are measured at B3LYP and B3PW91 methods. Comparing the electron density transitions from atomic lone pairs to bonding orbitals, it is obvious that the transitions from lone pairs of phosphoryl oxygen atoms to the π^* and σ^* of P=O, P–O, P–N bonds [Lp (O1) → π^* (P1–O1), Lp (O1) → σ^* (P1–O2), Lp (O1) → σ^* (P1–N1)] with the energies of about 650–750 kcal/mol are the most important interactions with the highest energies in isolated drugs **3** and **4**. The important electron density transitions from bonding to antibonding orbitals include σ (P1–O1) → σ^* (P1–O2) and σ (P1–O1) → σ^* (P1–N2), σ (P1–O1) → σ^* (N1–C3) with the energies of about 730–830 kcal/mol. These transitions display the charge transfers from the P=O to P–O/P–N bonds. Analogous data are observed for compound **4**. In complexes **12** and **13**, different results are achieved in which Lp1 (O1) → σ^* (P1–N1), Lp1 (O1) → σ^* (P1–N2) and Lp1 (O2) → σ^* (P1–N1), Lp1 (O2) → σ^* (P1–N2) are the most significant interactions with the energies of almost 590, 580 kcal/mol, respectively, indicating the charge transfer from the lone pairs of oxygen atoms O1, O2 to the P–N bonds. These differences in the electron density transitions of isolated drugs and their related complexes confirm the existence of interactions between C_{60} and drugs.

3.3. QTAIM analysis

An attractive aspect of this work is the topological study of electron density for free drug molecules and their corresponding complexes with C_{60} using QTAIM calculations. The QTAIM representations of compounds **3**, **12** and **4**, **13** are illustrated in Figs. 4 and 5, respectively, which are the collection of all critical points of B3LYP/6-31G(d) electron densities and their associated bond paths. The QTAIM analyses were performed by calculating the wave functions of electron densities for the optimized structures. The computed values of electron density ($\rho(\mathbf{r})$ in ea_0^{-3}), Laplacian of electron density ($\nabla^2\rho(\mathbf{r})$ in ea_0^{-5}), kinetic energy density ($G(\mathbf{r})$ in $e^2a_0^{-4}$), potential energy ($V(\mathbf{r})$ in $e^2a_0^{-4}$), total electronic energy density ($H(\mathbf{r})$ in $e^2a_0^{-4}$) and $|V(\mathbf{r})|/G(\mathbf{r})$ of some selected bond critical points (bcps) for compounds **3**, **4**, **12** and **13** are listed in Table 4.

Based on the QTAIM theory, the $\rho(\mathbf{r})$, $\nabla^2\rho(\mathbf{r})$ and $H(\mathbf{r})$ at a bcp provide information about the strength and characteristic of a bond. The large $\rho(\mathbf{r})$ value, $\nabla^2\rho(\mathbf{r}) < 0$ and $H(\mathbf{r}) < 0$ denote the covalent bond whereas small $\rho(\mathbf{r})$ values, $\nabla^2\rho(\mathbf{r}) > 0$ and $H(\mathbf{r}) > 0$ refer to closed-shell and ionic interactions [40,47]. In other words, values of $\rho(\mathbf{r}) < 0.1$ au are related to a closed-shell (mainly electrostatic) interaction [48] and are accompanied by a nearly small and positive value of $\nabla^2\rho(\mathbf{r})$ [49]. However, for a shared (mainly covalent) interaction, $\rho(\mathbf{r})$ is usually >0.1 au [49] and $\nabla^2\rho(\mathbf{r})$ is typically negative [50] and generally of the same order as $\rho(\mathbf{r})$. The $H(\mathbf{r})$ at a bcp, instead of $\nabla^2\rho(\mathbf{r})$, is a more proper index for better analyzing a weak interaction. The electronic energy density is obtained from the equation $H(\mathbf{r}) = G(\mathbf{r}) + V(\mathbf{r})$. The energy density term $G(\mathbf{r})$ is calculated according to equation $(1/4)\ \nabla^2\rho(\mathbf{r}) = 2G(\mathbf{r}) + V(\mathbf{r})$ [40].

It is apparent from Table 4 that the large electron densities for $\rho(\mathbf{r})$ values (0.1667–0.3267 ea_0^{-3}) at the bcps confirm the shared interaction for the P=O, P–O, P–N, C–O, C–N and N–H bonds in all compounds **3**, **4**, **12** and **13**. Although these polar bonds are covalent, positive $\nabla^2\rho(\mathbf{r})$ values (0.4512–1.6004 ea_0^{-5}) for bcps of the P=O, P–O and P–N bonds but negative $\nabla^2\rho(\mathbf{r})$ values (from −0.3795 to −1.6004 ea_0^{-5}) are obtained for bcps of the C–O, C–N and N–H bonds. Large electron density with large positive values for $\nabla^2\rho(\mathbf{r})$ both reveal a considerable stabilization of electron density near the interatomic surface and an electron density transfer to the more electronegative atom's basin resulting in depletion of electron density in the other atomic basin. Such results were also elucidated for CO and CS polar bonds by Bader [40,47]. Moreover, the electronic energy density values help more precise description of the nature of bonds. Thus, the negative $H(\mathbf{r})$ values in the range from −0.1080

to −0.4494 $e^2 a_0^{-4}$ are indicative of the predominant covalent character for the P=O, P–O, P–N, C–O, C–N and N–H bonds in all species.

Other important features of QTAIM calculations that can clearly be seen in Figs. 4b and 5b for complexes **12** and **13** are the presence of CH...HC intramolecular interactions or H...H dihydrogen bonds [51]. The small $\rho(\mathbf{r})$ values for the dihydrogen interactions (0.0048, 0.0050 $e a_0^{-3}$) and the positive values of $\nabla^2\rho(\mathbf{r})$, $H(\mathbf{r})$ at the bcps confirm the electrostatic nature of the CH...HC interactions. The presence of H...H bond results in formation of a seven-member ring in each compound. It is also evident from Figs. 4b and 5b that the interactions between C_{60} and compounds **3**, **4** are of electrostatic nature so that the small values for $\rho(\mathbf{r})$, $\nabla^2\rho(\mathbf{r})$ and $H(\mathbf{r})$ at the bcps of P1=O1...C7 confirm this issue.

There is one intramolecular CH...NH hydrogen bond and also two intermolecular electrostatic CH...C(fullerene) interactions in both complexes **12** and **13**. For all of these interactions, small positive values are measured for $\rho(\mathbf{r})$, $\nabla^2\rho(\mathbf{r})$ and $H(\mathbf{r})$ (Table 4) reflecting their ionic/electrostatic natures. The results confirm that there are electrostatic interactions between C_{60} and drugs, thus a physical sorption takes place. It is also valuable to note that it has been indicated that these kinds of intramolecular interactions (such as formation of H...H bonds) can have stabilizing effects on the structure [51].

It was found that the $|V(\mathbf{r})|/G(\mathbf{r})$ ratio (where $|V(\mathbf{r})|$ is the magnitude of $V(\mathbf{r})$) is a reliable parameter to categorize the interatomic interactions [52]. Based on this suggested parameter, closed-shell interactions are associated with $|V(\mathbf{r})|/G(\mathbf{r}) \leq 1$ (or $H(\mathbf{r}) = G(\mathbf{r}) + V(\mathbf{r}) \geq 0$), intermediate interactions $1 < |V(\mathbf{r})|/G(\mathbf{r}) < 2$, and shared interactions $|V(\mathbf{r})|/G(\mathbf{r}) > 2$. The calculated values of $|V(\mathbf{r})|/G(\mathbf{r})$ in Table 4 support the covalent/shared character of the C–O, C–N and N–H bonds, the intermediate character of P=O, P–O and P–N bonds while the electrostatic nature of P1=O1...C7, HC...HC, CH...NH, ClCH...C(fullerene), BrCH...C(fullerene), N2–H...C(fullerene) and CH...C(fullerene) interactions with their corresponding $|V(\mathbf{r})|/G(\mathbf{r})$ values are in the range of 2.4320–10.1820, 1.2745–1.5587 and 0.5712–0.8234, respectively.

3.4. NQR analysis

Selected calculated nuclear quadrupole coupling constants (NQCCs, χs) and asymmetry parameters (ηs) for the quadrupole nuclei ^{2}H, ^{14}N, ^{17}O, ^{35}Cl, ^{37}Cl, ^{79}Br and ^{81}Br of compounds **3**, **4**, **12** and **13** are presented in Table 5. It is observed that similar results are obtained at both B3LYP and B3PW91 levels. In all compounds, the exocyclic nitrogen atoms indicate greater χ values than endocyclic N atoms within the aliphatic six-membered ring. This may be attributed to the more positive charge exists on the exocyclic nitrogen leading to its stronger interaction with the electric field gradient. In addition, the oxygen atoms of P=O and P–O bonds have χ values about 5.0 and 10.0 MHz, respectively. The reason for the almost half χ values of oxygen atoms in phosphoryl moieties relative to those of P–O groups could be the much more positive oxygen atoms in P–O bonds that have a greater interaction with EFG tensor. Moreover, the asymmetry parameter values are about ten times greater for the endocyclic oxygen atoms that those of phosphoryl oxygen atoms. Thus, the great deviations from the spherical symmetry are expected to create stronger interactions between the EFG and quadrupole nuclei. The χ values for ^{14}N and ^{2}H were obtained about 5 MHz and 255 kHz, respectively. Comparable results have been reported for earlier studied phosphoramides [53]. The NQCCs for ^{35}Cl, ^{37}Cl, ^{79}Br and ^{81}Br nuclei are approximately 295, 230, 2080–2090 and 1735–1750 MHz, respectively.

4. Conclusion

In summary, physical adsorption of nine derivatives of the cyclophosphamide prodrug on the surface of C_{60} nanocage through the interaction of phosphoryl oxygen with a carbon atom of C_{60} was performed using DFT computations at B3LYP and B3PW91 levels of theory. A range of binding energies were measured for these systems so that complex **13** showed the most negative gCP-D3-$\Delta E_{binding}$ at the B3LYP level of theory. The NBO calculations demonstrated nearly identical band gaps for C_{60} and complexes **11**–**19** ($E_g \approx 2.7$ eV) but higher values for the isolated drugs (6.5–8.0 eV). According to $|V(\mathbf{r})|/G(\mathbf{r})$ ratios, the C–O, C–N, N–H bonds, P=O, P–O, P–N bonds and P1=O1...C7, HC...HC, CH...NH, ClCH...C(fullerene), BrCH...C(fullerene), N2–H...C(fullerene), CH...C(fullerene) interactions have covalent/shared, intermediate and electrostatic natures, respectively. Finally, it can be said that the complexes **12** and **13** are expected to work the best as drug delivery systems because of their greatest binding energies among the complexes.

Acknowledgements

The financial support of this work by Research Council of Amirkabir University of Technology (Polytechnic) is gratefully acknowledged. We are indebted to Center of Excellence on Computational Aerospace Engineering (AEROEXCEL) at Amirkabir University of Technology and particularly to Mr. Eshraghi and Dr. Karimian for providing supercomputers. The authors also would like to thank Mr. Cheraghchi, Miss Molaee and especially Professor C.O.D. Védova for their great help in providing computer services (hardwares and softwares).

Appendix A. Supplementary data

Supplementary material related to this article can be found, in the online version, at http://dx.doi.org/10.1016/j.jmgm.2014.06.001.

References

[1] H.W. Kroto, J.R. Heath, S.C. O'Brien, R.F. Curl, R.E. Smalley, C60: Buckminsterfullerene, Nature 318 (1985) 162–163.
[2] W. Krätschmer, L.D. Lamb, K. Fostiropoulos, D.R. Huffiman, Solid C_{60}: a new form of carbon, Nature 347 (1990) 354–358.
[3] S.H. Friedman, D.L. DeCamp, R.P. Sijbesma, G. Srdanov, F. Wudl, G.L. Kenyon, Inhibition of the HIV-1 protease by fullerene derivatives: model building studies and experimental verification, J. Am. Chem. Soc. 115 (1993) 6506–6509.
[4] D.M. Guldi, M. Prato, Excited-state properties of C_{60} fullerene derivatives, Acc. Chem. Res. 33 (2000) 695–703.
[5] M.C. DeRosa, R.J. Crutchley, Photosensitized singlet oxygen and its applications, Coord. Chem. Rev. 233 (2002) 351–371.
[6] D.W. Cagle, S.J. Kennel, S. Mirzadeh, J.M. Alford, L.J. Wilson, In vivo studies of fullerene-based materials using endohedral metallofullerene radiotracers, Proc. Natl. Acad. Sci. U.S.A. 96 (1999) 5182–5187.
[7] M. Lucafò, S. Pacor, C. Fabbro, T. Da Ros, S. Zorzet, M. Prato, G. Sava, Study of a potential drug delivery system based on carbon nanoparticles: effects of fullerene derivatives in MCF7 mammary carcinoma cells, J. Nanopart. Res. 14 (2012) 830–838.
[8] A. Montellano, T. Da Ros, A. Bianco, M. Prato, Fullerene C 60 as a multifunctional system for drug and gene delivery, Nanoscale 3 (2011) 4035–4041.
[9] L.L. Dugan, D.M. Turetsky, C. Du, D. Lobner, M. Wheeler, C.R. Almli, C.K.F. Shen, T.-Y. Luh, D.W. Choi, T.-S. Lin, Proc. Natl. Acad. Sci. U.S.A. 94 (1997) 9434–9439.
[10] C.M. Sayes, A.A. Marchione, K.L. Reed, D.B. Warheit, Comparative pulmonary toxicity assessments of C60 water suspensions in rats: few differences in fullerene toxicity in vivo in contrast to in vitro profiles, Nano Lett. 7 (2007) 2399–2406.
[11] Z. Markovic, V. Trajkovic, Biomedical potential of the reactive oxygen species generation and quenching by fullerenes (C60), Biomaterial 29 (2008) 3561–3573.
[12] M.Y. Song, G.B. Jiang, J.F. Yin, H.L. Wang, Inhibition of polymerase activity by pristine fullerene nanoparticles can be mitigated by abundant proteins, Chem. Commun. 46 (2010) 1404–1406.

[13] A. Trpkovic, B. Todorovic-Markovic, V. Trajkovic, Toxicity of pristine versus functionalized fullerenes: mechanisms of cell damage and the role of oxidative stress, Arch. Toxicol. 86 (2012) 1809–1827.
[14] S. Deguchi, R.G. Alargova, K. Tsujii, Stable dispersions of fullerenes, C60 and C70, in water preparation and characterization, Langmuir 17 (2001) 6013–6017.
[15] Y. Liu, H. Wang, P. Liang, H.Y. Zhang, Water-soluble supramolecular fullerene assembly mediated by metallobridged β-cyclodextrins, Angew. Chem. Int. Ed. 43 (2004) 2690–2694.
[16] H. Tokuyama, S. Yamago, E. Nakamura, T. Shiraki, Y. Sugiura, Photoinduced biochemical activity of fullerene carboxylic acid, J. Am. Chem. Soc. 115 (1993) 7918–7919.
[17] A. Ikeda, M. Yoshimura, S. Shinkai, Solution complexes formed from C60 and calixarenes. On the importance of the preorganized structure for cooperative interactions, Tetrahedron Lett. 38 (1997) 2107–2710.
[18] Z. Yoshida, H. Takekuma, S. Takekuma, Y. Matsubara, Molecular recognition of C60 with γ-cyclodextrin, Angew. Chem. Int. Ed. Engl. 33 (1994) 1597–1599.
[19] L. Xiao, H. Takada, H. Gan Xue, N. Miwa, The water-soluble fullerene derivative "Radical Sponge" exerts cytoprotective action against UVA irradiation but not visible-lightcatalyzed cytotoxicity in human skin keratinocytes, Bioorg. Med. Chem. Lett. 16 (2006) 1590–1595.
[20] Y. Iwamoto, Y. Yamakoshi, A highly water-soluble C60-NVP copolymer: a potential material for photodynamic therapy, Chem. Commun. (2006) 4805–4807.
[21] T. Andersson, K. Nilsson, M. Sundahl, G. Westman, O. Wennerstroem, C60 embedded in γ-cyclodextrin: a water-soluble fullerene, J. Chem. Soc. Chem. Commun. (1992) 604–606.
[22] S.M. Rezayat, S.V.S. Boushehri, B. Salmanian, A.H. Omidvari, S. Tarighat, S. Esmaeili, S. Sarkar, N. Amirshahi, R.N. Alyautdin, M.A. Orlova, I.V. Trushkov, A.L. Buchachenko, K.C. Liu, D.A. Kuznetsov, The porphyrin–fullerene nanoparticles to promote the ATP overproduction in myocardium: 25Mg2þ-magnetic isotope effect, Eur. J. Med. Chem. 44 (2009) 1554–1569.
[23] D.V. Konareva, S.S. Khasanov, R.N. Lyubovskaya, Fullerene complexes with coordination assemblies of metalloporphyrins and metal phthalocyanines, Coord. Chem. Rev. 262 (2014) 16–36.
[24] C. Dumitriu, Z. Mousavi, R.-M. Latonen, J. Bobacka, I. Demetrescu, Electrochemical synthesis and characterization of poly(3,4-ethylenedioxythiophene) doped with sulfonated calixarenesand sulfonated calixarene–fullerene complexes, Electrochim. Acta 107 (2013) 178–186.
[25] S.A. Mizyed, E. Al-Jarrah, D. Marji, M. Ashram, A spectrophotometric study of the charge transfer complexes of [60]fullerene with different tert-butylcalix[4]crowns, Spectrochim. Acta Part A 68 (2007) 1274–1277.
[26] N. Amirshahi, R.N. Alyautdin, S. Sarkar, S.M. Rezayat, M.A. Orlova, I.V. Trushkov, A.L. Buchachenko, D.A. Kuznetsov, Fullerene-based low toxic nanocationite particles (porphyrin adducts of cyclohexyl fullerene-C60) to treat hypoxia-induced mitochondrial dysfunction in mammalian heart muscle, Arch. Med. Res. 39 (2008) 549–559.
[27] S. Tollas, I. Bereczki, A. Sipos, E. Rőth, G. Batta, L. Daróczi, S. Kéki, E. Ostorházi, F. Rozgonyi, P. Herczegh, Nano-sized clusters of a teicoplanin ψ-aglycon-fullerene conjugate. Synthesis, antibacterial activity and aggregation studies, Eur. J. Med. Chem. 54 (2012) 943–948.
[28] Z. Wang, J. Zhang, DFT study on structural, electronic, and vibrational properties of the highest oxygenated fullerene $C_{24}O_{12}$, Comput. Theor. Chem. 972 (2011) 20–24.
[29] H. Tachikawa, T. Iyama, S. Abe, DFT study on the interaction of Fullerene (C60) with hydroxyl radical (OH), Phys. Proc. 14 (2011) 139–142.
[30] B. Barszcz, B. Laskowska, A. Graja, E.Y. Park, T.-D. Kim, K.-S. Lee, Electronic excitations of the fullerene–thiophene-derived dyads, Syn. Met. 161 (2011) 229–234.
[31] Y.-H. Kim, Y. Zhao, A. Williamson, M.J. Heben, S.B. Zhang, Nondissociative adsorption of H_2 molecules in light-element-doped fullerenes, Phys. Rev. Lett. 96 (2006) 016102–016104.
[32] R.F. Borch, J.A. Millard, J. Med. Chem. 30 (1987) 427–431.
[33] B.E.P.J. Vriens, M.J.B. Aarts, B. de Vries, S.M. van Gastel, J. Wals, T.J. Smilde, L.J.C. van Warmerdam, M. de Boer, D.J. van Spronsen, G.F. Borm, V.C.G. Tjan-Heijnen, Breast Cancer Trialists' Group of the Netherlands (BOOG), Doxorubicin/cyclophosphamide with concurrent versus sequential docetaxel as neoadjuvant treatment in patients with breast cancer, Eur. J. Cancer 49 (2013) 3102–3110.
[34] L. Thoenes, M. Hoehn, R. Kashirin, M. Ogris, G.J. Arnold, E. Wagner, M. Guenther, In vivo chemoresistance of prostate cancer in metronomic cyclophosphamide therapy, J. Proteomics 73 (2010) 1342–1354.
[35] G. Sanna, M. Pestrin, E. Zafarana, C. Biagioni, D. Cavaciocchi, N. Turner, A. Di Leo, L. Biganzoli, Feasibility and safety of dose-dense docetaxel after conventional epirubicin and cyclophosphamide as adjuvant treatment for early breast cancer patients, Breast 22 (2013) 926–932.
[36] M.C. Liu, G.D. Demetri, D.A. Berry, L. Norton, G. Broadwater, N.J. Robert, D. Duggan, D.F. Hayes, I.C. Henderson, A. Lyss, J. Hopkins, P.A. Kaufman, P.K. Marcom, J. Younger, N. Lin, K. Tkaczuk, E.P. Winer, C.A. Hudis, for the Cancer and Leukemia Group B, Dose-escalation of filgrastim does not improve efficacy: clinical tolerability and long-term follow-up on CALGB study 9141 adjuvant chemotherapy for node-positive breast cancer patients using dose-intensified doxorubicin plus cyclophosphamide followed by paclitaxel, Cancer Treat. Rev. 34 (2008) 223–230.
[37] M.J. Frisch, G.W. Trucks, H.B. Schlegel, G.E. Scuseria, M.A. Robb, J.R. Cheeseman, V.G. Zakrzewski, J.A. Montgomery, R.E.J. Stratmann Jr., C. Burant, S. Dapprich, J.M. Millam, A.D. Daniels, K.N. Kudin, M.C. Strain, O. Farkas, J. Tomasi, V. Barone, M. Cossi, R. Cammi, B. Mennucci, C. Pomelli, C. Adamo, S. Clifford, J. Ochterski, G.A. Petersson, P.Y. Ayala, Q. Cui, K. Morokuma, D.K. Malick, A.D. Rabuck, K. Raghavachari, J.B. Foresman, J. Cioslowski, J.V. Ortiz, A.G. Baboul, B.B. Stefanov, G. Liu, A. Liashenko, P. Piskorz, I. Komaromi, R. Gomperts, R.L. Martin, D.J. Fox, T. Keith, M.A. Al-Laham, C.Y. Peng, A. Nanayakkara, M.P. Challacombe, M.W. Gill, B. Johnson, W. Chen, M.W. Wong, J.L. Andres, C. Gonzalez, M. Head-Gordon, E.S. Replogle, J.A. Pople, Gaussian 98, Revision A9, Gaussian, Inc., Pittsburgh, PA, 1998.
[38] R. Bersohn, Nuclear electric quadrupole spectra in solids, J. Chem. Phys. 20 (1952) 1505–1509.
[39] P. Pyykö, Spectroscopic nuclear quadrupole moments, Mol. Phys. 99 (2001) 1617–1629.
[40] R.F.W. Bader, Atoms in Molecules: A Quantum Theory, Oxford University Press, Oxford, UK, 1990.
[41] R.F.W. Bader, AIM2000 Program ver 2.0, McMaster University, Hamilton, 2000.
[42] H. Kruse, L. Goerigk, S. Grimme, Why the standard B3LYP/6-31G* model chemistry should not be used in DFT calculations of molecular thermochemistry: understanding and correcting the problem, J. Org. Chem. 77 (2012) 10824–10834.
[43] K. Gholivand, M.Z. Pourayoubi, Z. Shariatinia, ^{2,3}J(P,X) [X = H C] coupling constants dependency on the ring size, hybridization and substituents in new diazaphospholes and diazaphosphorinanes, NMR and X-ray crystallography studies, Polyhedron 26 (2007) 837–844.
[44] W. Renxiao, F. Ying, L. Luhua, A new atom-additive method for calculating partition coefficients, J. Chem. Inf. Comput. Sci. 37 (1997) 615–621.
[45] D.E.C. Corbridge, Phosphorus, an Outline of Its Chemistry, Biochemistry and Technology, 5th Ed., Elsevier, the Netherlands, 1995.
[46] Z. Shariatinia, H.S. Mirhosseini Mousavi, P.J. Bereciartua, M. Dusek, Structures of a novel phosphoric triamide and its organotin(IV) Complex, J. Organomet. Chem. 745–746 (2013) 432–438.
[47] R.F.W. Bader, A quantum theory of molecular structure and its applications, Chem. Rev. 91 (1991) 893–928.
[48] R.F.W. Bader, H. Essén, The characterization of atomic interactions, J. Chem. Phys. 80 (1983) 1943–1960.
[49] R.G.A. Bone, R.F.W. Bader, Identifying and analyzing intermolecular bonding interactions in van der Waals molecules, J. Phys. Chem. 100 (1996) 10892–10911.
[50] M.F. Bobrov, G.V. Popova, V.G. Tsirelson, A topological analysis of electron density and chemical bonding in cyclophosphazenes PnNnX2n (X = H, F, Cl; N = 2, 3, 4), Russ. J. Phys. Chem. 80 (2006) 584–590.
[51] C.F. Matta, J. Hernandez-Trujillo, T.H. Tang, R.F.W. Bader, Hydrogen–hydrogen bonding: a stabilizing interaction in molecules and crystals, Chem. Eur. J. 9 (2003) 1940–1951.
[52] E. Espinosa, I. Alkorta, J. Elguero, E. Molins, From weak to strong interactions: a comprehensive analysis of the topological and energetic properties of the electron density distribution involving X–H. . .F–Y systems, J. Chem. Phys. 117 (2002) 5529–5542.
[53] Z. Shariatinia, C.O.D. Védova, M.F. Erben, V. Tavasolinasab, K. Gholivand, Synthesis, conformational and NQR analysis of phosphoric triamides containing the P(O)[N]3 skeleton, J Mol. Struct. 1023 (2012) 18–24.